J Porous Mater
DOI 10.1007/s10934-014-9896-2

Adsorption of methylene blue and Orange II pollutants on activated carbon prepared from banana peel

Jianfeng Ma · Daiqin Huang · Jing Zou · Liangyin Li · Yong Kong · Sridhar Komarneni

Abstract Banana peel-activated carbon (BPAC) with a very high surface area of 1,950 m^2 g^{-1} was prepared and investigated for the removal of methylene blue (MB) or Orange II dye molecules from aqueous solutions. Results of adsorption experiments showed that the BPAC exhibited high adsorption capacity with cationic dyes. The maximal Orange II and MB uptakes were determined to be more than 333 and 1,263 mg g^{-1}, respectively. The zeta-potential analysis revealed that surface charge of BPAC is negative and hence the present activated carbon is excellent for adsorption of MB cationic dye from water. The adsorption equilibrium, kinetics, and thermodynamics of MB dye were investigated and the results indicated a monolayer chemical adsorption involving electrostatic attraction. BPAC was found to be a highly promising material for the effective removal of cationic contaminants such as MB dye from water.

Keywords Activated carbon · Dye pollutants · Methylene blue cationic dye · Orange II anionic dye · Adsorption

1 Introduction

With the recent enormous industrialization of especially developing countries, water pollution has become a serious problem. The primary water pollutants that adversely affect biological diversity, ecosystem function, and the natural processes of aquatic systems include all kinds of hazardous organic molecules and inorganic chemical species. For example, one such hazardous pollutant is azo dye [1]. Azo dyes are known to be toxic to aquatic organisms and carcinogenic and mutagenic to humans. Therefore, effective approaches must be developed to remove azo dyes from waste water before its discharge into the environment. The existing techniques to remove dyes from dye-containing waste water include chemical coagulation/flocculation [2, 3], ozonation [4], oxidation processes including electroperoxone treatment [5, 6], ion exchange [7] and ultrafiltration [8]. However, these techniques have some disadvantages and limitations, such as high cost [9], generation of secondary pollutants, and intensive energy requirements. Although adsorption processes using activated carbons have been found to be effective in the treatment of these waste waters [10, 11], the preparation and regeneration of activated carbons are relatively costly, thus limiting their application. Therefore, interest in the production of activated carbons from low-cost organic waste materials for dye removal has increased considerably. Several nonconventional bio-based products were previously used by others [12–19] to prepare activated carbon adsorbents and were studied for their ability to remove dyes from aqueous solutions. Examples of these bio-based products included oil palm empty fruit bunch fibers [12], hevea brasiliensis seed coat [13], swede rape straw (*Brassica napus* L.) [14], cocoa (*Theobroma cacao*) shell [15], waste apricot [16], olive cake [17], succinylated sugarcane bagasse [18], and *Chaetophora* algae [19]. Activated carbons are widely used adsorbent materials with meso to microporous characteristics and they have an advantage over other adsorbents in terms of the cost of

J. Ma · D. Huang · J. Zou · L. Li · Y. Kong
School of Environmental and Safety Engineering, Changzhou University, Jiangsu 213164, China

J. Ma · S. Komarneni (✉)
Materials Research Laboratory, Materials Research Institute, The Pennsylvania State University, University Park, PA 16802, USA
e-mail: sxk7@psu.edu; komarneni@psu.edu

Published online: 16 December 2014

precursor materials for their production. A wide variety of organic sources are available for the production of activated carbons and hence industrial production is expected to be cost-effective [20].

Banana peel is a lignocellulosic and low-cost agricultural waste residue that is readily available in large quantities. In this study, banana peel was used as a renewable precursor for activated carbon preparation for dye removal. The results of this study would help in preparing value-added product from one of the agricultural wastes and present a cost-effective alternative to existing commercially available activated carbons. To the best of our knowledge, no report has documented the use of banana peel-activated carbon (BPAC) as a low-cost alternative adsorbent for MB or Orange II removal from wastewater. The primary purpose of the present research is to evaluate the adsorption potential of BPAC for dye removal. Textural, functional, and surface characterization of the prepared BPAC adsorbent was performed. The adsorption equilibrium, isotherms, kinetics, mechanism, and thermodynamics of MB dye adsorption were determined and presented here for potential use of this new BPAC adsorbent to clean up toxic dyes from water.

2 Materials and methods

2.1 Chemicals

Potassium hydroxide (KOH) and hydrochloric acid (HCl) used in this study were purchased from the Sinopharm Chemical Reagent Co., Ltd, China. They were both of analytical grade and were used as received without further purification. Cationic MB (analytical grade, $C_{16}H_{18}ClN_3S \cdot H_2O$, $\lambda_{max} - 665$ nm) supplied by Shanghai Lunjie Chemical Reagent Co., Ltd. (China) and anionic Orange II (analytical grade, $C_{16}H_{11}N_2NaO_4S$, $\lambda_{max} - 485$ nm) supplied by Sinopharm Chemical Reagent Co., Ltd. (China) were chosen as the dye molecules for determining their adsorption on BPAC and were used without any purification. Distilled water was used to prepare the desired concentrations of dye solutions.

2.2 Adsorbents

The banana peels used for the preparation of activated carbon were obtained from a local source in Changzhou, China. The precursor was first washed with distilled water and dried overnight at 105 °C to remove moisture. It was then cut, ground and sieved to pass through a 100 mesh sieve, and the obtained powder was labeled as original banana peel (OBP). Then the powder was carbonized in a combustion boat placed in a tube furnace in vacuum at 500 °C with a heating rate of 5 °C/min. The sample was held at the carbonization temperature for 4 h. A certain amount of thus produced char was then soaked with KOH solution at an impregnation weight ratio of 2:1 (KOH:-char). The mixture was dehydrated in an oven overnight at 105 °C to remove moisture. It was then activated under the same conditions which were used above for carbonization but at a final temperature of 750 °C for 2 h. The activated product was then cooled under vacuum to room temperature and then washed with deionized water and 0.1 M HCl until the pH of the washing solution reached 6–7. After washing, the BPAC was dried at 105 °C in a drying oven for 5 h and the dried BPAC was stored in a sample bottle before further use in various experiments.

2.3 Characterization methods

The morphologies of the different samples were characterized by using a scanning electron microscope (SEM, Hitachi S4800, Japan). The Brunauer–Emmett–Teller (BET) surface area and porous property of the OBP and the BPAC were measured by determining the N_2 adsorption isotherm at −196 °C with an adsorption analyzer (NOVA, 2000E, Quantachrome, USA). Prior to adsorption, the samples were degassed in a vacuum at 120 °C for 12 h. The relative pressure (P/P_0) between 0.05 and 0.35 was applied for the calculation of BET-N_2 surface areas. The total pore volumes of the samples were calculated at $P/P_0 = 0.98$. The surface area (S_{BET}) and the total pore volume (V_{tot}) were obtained by using the manufacturer's software. The specific surface area was derived from BET theory. The micropore surface area (S_{mic}), the external surface area (S_{ext}), and the micropore volume (V_{mic}) were evaluated by the t-plot method. The pore size distribution was obtained by using the density functional theory method. The mean pore diameter (D_p) was obtained from $D_P = 4V_{tot}/S_{BET}$. The Fourier transform infrared (FTIR) spectra were obtained using the KBr pressed disk technique on a Thermo Nicolet Nexus 670 FTIR spectrophotometer. The FTIR spectra ranging from 4,000 to 400 cm^{-1} were recorded with a resolution of 4 cm^{-1} and 64 interferograms were collected. The zeta potentials of OBP and BPAC in aqueous solution were determined using a Zetasizer 3000 HSA (Malvern Instruments).

2.4 Batch adsorption experiments

For equilibrium measurements, batch adsorption experiments of dyes (MB or Orange II) on OBP or BPAC were performed using 50 mL centrifuge tubes that contain a definite volume (20 mL in each tube) of fixed initial concentrations of dye solution. The tubes were capped and placed on an orbital shaker at 180 rpm for 5 h to ensure

apparent equilibrium. After shaking, the sample and solutions were centrifuged at 3,500 rpm for 10 min to separate solutions from solids. Subsequent to centrifugation, aliquots of the supernatants were collected and used to determine the concentrations of the remaining dye. The amount of adsorbate adsorbed at equilibrium condition, q_e (mg g^{-1}), was calculated by the following equation:

$$q_e = \frac{(C_0 - C_e)\, v}{m} \tag{1}$$

where C_0 and C_e (mg L^{-1}) are the initial and equilibrium dye concentrations, respectively. V(L) is the volume of the solution, and m (g) is the mass of adsorbent used. Duplicate experiments were carried out for all the operating variables studied.

For kinetic measurements, the experiments were carried out using three different initial MB dye concentrations (800, 1,000, and 1,200 mg L^{-1}) with a fixed adsorbent concentration i.e., adsorbent/solution ratio of 2.5 g L^{-1} at room temperature. For kinetics studies, solutions were collected at predefined time intervals and the concentrations of the dye were determined. Distilled water was used to prepare standard solutions of different concentrations of dye solutions, and a spectrophotometer (UV-2450, Shimadzu) was employed to measure the concentration of dye at λ_{max} using a standard calibration curve.

To study the effect of temperature on the adsorption characteristics, the adsorption experiments were conducted by determining the adsorption isotherms at 298, 308 and 318 K using dye concentrations varying from 1,000 to 2,000 mg L^{-1}. All other variables, such as the activated carbon dose and contact time remained constant. The initial solution pH values during all the above adsorption experiments were in the range of 6.3–6.9. However, their solution pH was not adjusted during the experiments.

3 Results and discussion

3.1 Adsorption isotherms of dye contaminants

The isotherm data on the adsorption of MB and Orange II dyes on OBP or BPAC adsorbents at various initial concentrations are presented in Fig. 1. Adsorption isotherm models, such as Langmuir and Freundlich [21], were fitted to the experimental data so as to determine the physicochemical properties of the adsorbents. The adsorption and model parameters are listed and compared in Table 1. Comparing the R^2 values of the two isotherms tested, the adsorption data fitted the Langmuir model satisfactorily with an R^2 value of >0.99.

The generalized Langmuir isotherm can be represented as follows:

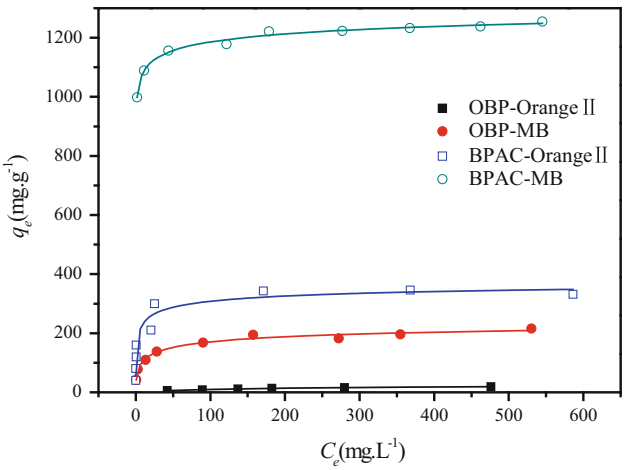

Fig. 1 Adsorption isotherms of MB and OrangeII on original banana peel (OBP) and banana peel activated carbon (BPAC)

$$\frac{C_e}{q_e} = \frac{C_e}{q_m} + \frac{1}{q_m b} \tag{2}$$

where C_e is the equilibrium concentration (mg L^{-1}), q_e is the amount of adsorbate adsorbed per unit mass of adsorbent at equilibrium (mg g^{-1}), q_m is the theoretical maximum adsorption capacity (mg g^{-1}), and b is the Langmuir isotherm constant related to the energy of adsorption (L mg^{-1}). A plot of C_e/q_e against C_e results in a straight line with a slope of $1/1q_m$ and an intercept of $1/1q_m\, b$.

The Freundlich equation is given as

$$\log q_e = \frac{1}{n} \log C_e + \log K_F \tag{3}$$

where K_F and n are Freundlich constants related to adsorption capacity and adsorption intensity, respectively. These parameters can be calculated from the intercept and the slope of the linear plot log q_e versus log C_e.

The values of q_m for MB and Orange II on BPAC are 333 and 1,263 mg g^{-1}, respectively, whereas the adsorption values on OBP are only 25 and 250 mg g^{-1}, respectively, under the same conditions (Table 1). The adsorption capacity considerably increased when OBP was modified into BPAC, as expected because BPAC has a very high surface area of 1,950 m^2 g^{-1}, which is largely due to microporous surface area (Table 2). In order to compare the adsorption capacity of BPAC, the adsorption capacities of some other activated carbons for MB or Orange II adsorption are included: the adsorption capacity of water hyacinth activated with H_3PO_4 for MB is 124 mg g^{-1} [22]; the adsorption capacity of buriti shell activated with $ZnCl_2$ for MB is 288.23 mg g^{-1} [23]; the adsorption capacity of commercial activated carbon fiber ACFT for Orange II is 230 mg g^{-1} [24]. These adsorption capacities are lower than the banana peel activated carbons produced in the

Table 1 Isotherm parameters obtained for the adsorption of MB and Orange II onto OBP or BPAC at different temperatures

Isother models	OBP		BP			
	Orange II	MB	Orange II	MB		
	298 K	298 K	298 K	298 K	308 K	318 K
Langmuir						
q_m (mg g^{-1})	25.00	250.00	333.33	1,262.77	1,287.28	1,293.01
b (L mg^{-1})	0.0065	0.0571	0.7500	0.1936	0.2312	0.2402
R_L	0.2353	0.0214	0.0013	0.0026	0.0022	0.0021
R^2	0.9910	0.9930	0.9990	0.9998	0.9998	0.9999
Freundlich						
K_F	1.1123	67.0509	142.7199	985.1461	991.0153	1,001.666
n	2.1468	5.2707	6.6124	25.9538	24.03846	24.55193
R^2	0.9637	0.9541	0.8876	0.9818	0.9811	0.9851

Table 2 Surface area and porosity values of the original banana peel (OBP) and banana peel activated carbon (BPAC)

	S_{BET} (m^2 g^{-1})	S_{mic}		S_{ext}		V_{tot} (cm^3 g^{-1})	V_{mic}		D_p (nm)
		(m^2 g^{-1})	(%)	(m^2 g^{-1})	(%)		(cm^3 g^{-1})	(%)	
OBP	0.0258	–	–	0.101	–	0.0003	–	–	44.614
BPAC	1,950	1,719	88.2	231	11.8	1.071	0.869	81.1	2.197

– Not analyzed

present study. Therefore, it seems that BPAC is an attractive candidate for removal of MB or Orange II from aqueous solution.

The SEM images of OBP and BPAC (Fig. 2a, b) show that the surface morphology of BPAC is rougher than that of OBP. This difference is attributable to the large number of volatile organic compounds that undergo pyrolysis and hence the original morphology was changed during carbonization or activation. Hence, many concave and convex creases, defects, and highly complex surface features of BPAC resulted. These features may provide access to the numerous micropores created throughout the activated carbon material during carbonization and activation. The microporous surface area is very large (Table 2), leading to very high adsorption of dye molecules.

Figure 3 shows the N_2 adsorption/desorption isotherms and the pore size distribution of the BPAC. According to the International Union of Pure and Applied Chemistry (IUPAC) classification of adsorption isotherms [25], the adsorption and desorption isotherms of N_2 at −196 °C for the BPAC are clearly a type I, which is a characteristic of microporous solids (Fig. 3). The isotherm plots exhibited a round knee indicating high adsorption capacity and wide distribution of micropores in microporous solids [26]. The

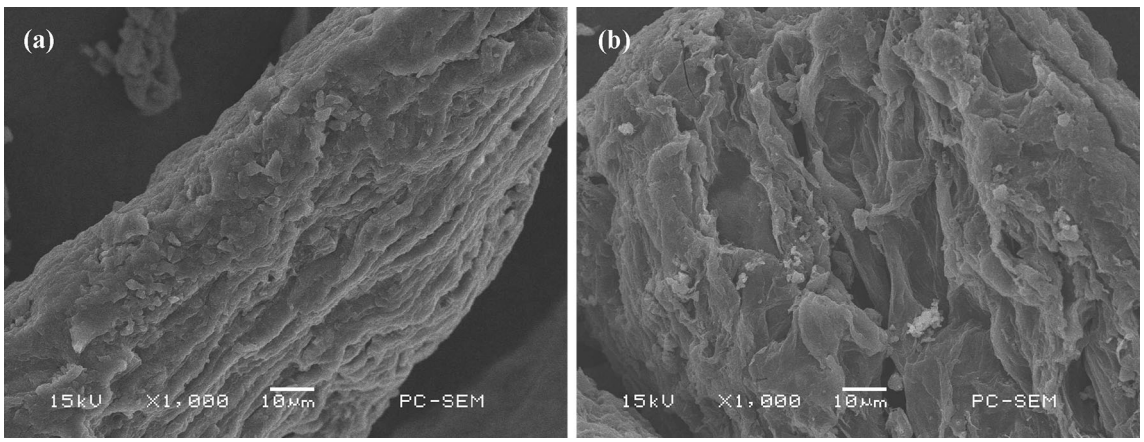

Fig. 2 SEM micrograhs of the original banana peel (**a**) and banana peel activated carbon (**b**)

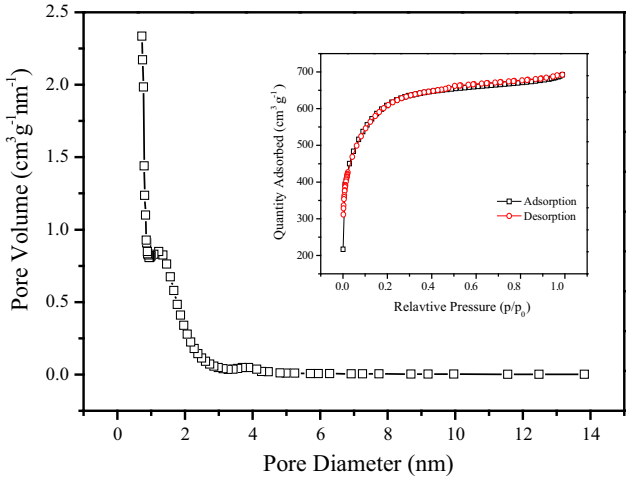

Fig. 3 Pore size distribution of banana peel activated carbon (BPAC) and the *inset figure* shows N_2 adsorption–desorption isotherms

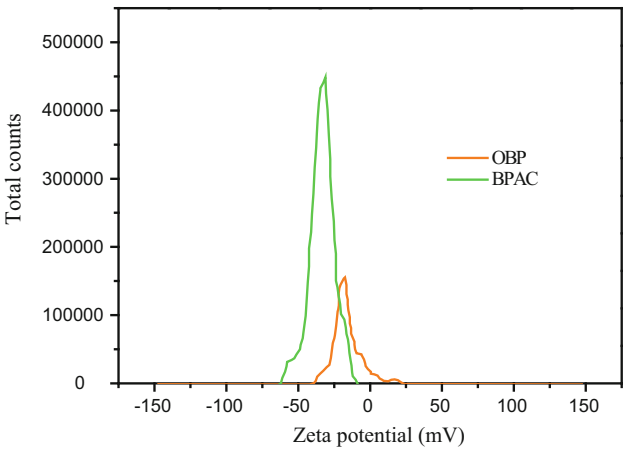

Fig. 4 Zeta potential distributions of original banana peel (OBP) and banana peel activated carbon (BPAC)

surface area and pore volume of OBP and BPAC were calculated and are listed in Table 2. As shown in Table 2, the surface area of BPAC is 1,950 $m^2\ g^{-1}$, which is extremely larger than that of the OBP, as expected. Thus the BPAC synthesized here is a very high surface area adsorbent and is much better than previously synthesized other adsorbents such as *Hevea brasiliensis* seed coat-derived activated carbon fiber with 1,225 $m^2\ g^{-1}$ [13] and *Phragmites australis*-derived activated carbon fiber with 1,362 $m^2\ g^{-1}$ [27]. The pore volume is 1.071 $cm^3\ g^{-1}$ while the micropore volume is 0.869 $cm^3\ g^{-1}$, which indicates that the newly obtained BPAC is mainly microporous (Table 2; Fig. 3). Although the experimental average pore diameter determined here was about 2.197 nm (Table 2), this activated BPAC can be considered as microporous because it is very close to the upper limit of 2 nm of micropores within experimental errors (Table 2; Fig. 3).

The adsorption of MB on OBP or BPAC was significantly better than that of Orange II (Table 1; Fig. 1). In order to explain the different adsorption behaviors of the two dyes, the zeta potential distribution of OBP and BPAC in aqueous solutions were determined (Fig. 4). The surface charges of OBP and BPAC are −16.2 and −33.8 mV (Fig. 4). The adsorption of anionic Orange II is not favorable on these adsorbents because of the electrostatic repulsion between the negatively charged OBP or BPAC surface and the negatively charged Orange II dye anion. However, MB is a positively charged cationic dye, which can easily adsorb on the negatively charged surface of OBP or BPAC through electrostatic attraction. Hence, the uptake of MB dye was found to be much higher than that of Orange II dye.

All the correlation coefficients, the R^2 values, and the constants of MB adsorption on BPAC obtained from the two isotherm models are summarized in Table 1. The Langmuir isotherm model provides the highest R^2 values, which were greater than 0.99 under all the temperatures studied. This result indicates the applicability of the Langmuir isotherm for MB adsorption onto BPAC. The essential characteristics of the Langmuir isotherm can be expressed in terms of dimensionless equilibrium parameter (R_L) [28] defined as

$$R_L = \frac{1}{(1 + bC_0)} \tag{4}$$

where C_0 is the highest initial dye concentration in the solution, R_L is a dimensionless separation factor and is used to confirm the favorability of the adsorption process, that is, $(0 < R_L < 1)$ is favorable, $R_L = 1$ is linear, $R_L = 0$ is irreversible, and $R_L > 1$ is unfavorable. The values of R_L obtained at various temperatures and reported in Table 1 were <1, thus indicating that the adsorption of MB dye onto BPAC is favorable.

In view of the adsorption mechanism at the molecular level, the Langmuir model suggests the facile anchoring of dye to the abundant functional groups of BPAC with the formation of monolayer surface coverage.

The FTIR spectra are of great help to get information about the chemical structure and functional groups of OBP, BPAC, MB, and BPAC after adsorption of MB. Figure 5 shows the FTIR spectra of these samples. Some peaks disappeared or decreased in intensity in BPAC relative to OBP. The peak at around 3,346 cm^{-1}, which is attributed to O–H stretching vibration of hydroxyl functional groups including hydrogen bonding, was much lower in BPAC. The bands at approximately 2,925 and 2,854 cm^{-1}, which are assigned to the stretching vibrations of methylene (C–H) in alkane groups, were lower in BPAC, indicating that activation removed a large amount of hydrogen. The peak at 1,735 cm^{-1} represents the stretching vibrations of

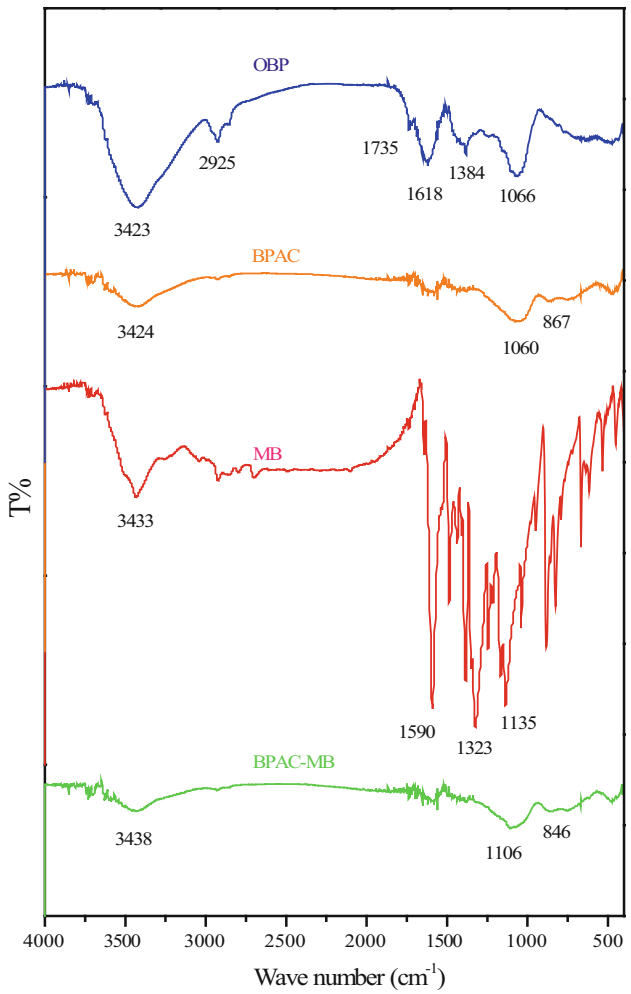

Fig. 5 FTIR spectra of original banana peel (OBP), banana peel activated carbon (BPAC), MB dye and BPAC adsorbed with MB

carbonyl double bond (C=O) that may be attributed to the lignin aromatic groups. Absorbance at 1,618 and 1,384 cm^{-1} corresponds to the C–N (or N–H) and C–H groups, respectively. The weak absorption peak at 1,238 cm^{-1} may represent the stretching vibrations of C–O–S in sulfate groups. The peak at 1,066 cm^{-1} is characteristic of the carbon–oxygen single bond (C–O) in alcohol or carbohydrates in the cell wall. A significant reduction was observed for a series of complex bands in the range of 1,066–1,735 cm^{-1} in BPAC, which comprises banana peel lipids, polysaccharides, and other substances of a specific functional group, indicating that chemical activation broke many aliphatic and aromatic bonds and eliminated much of the volatile matter. As shown in Fig. 5, the spectral analysis of BPAC before and after MB dye adsorption reveals many clusters of small peaks that range from 1,800 to 1,690 cm^{-1} representing C=O groups and from 1,675 to 1,640 cm^{-1} representing C=C groups [15]). Analysis of the spectra also indicates that most bonded O–H, stretched C–O, and C–H groups were involved in MB dye adsorption. After adsorption, the band shifts were clear, and an intense decrease in the band of BPAC-MB could be noted at 3,424, 1,060, and 867 cm^{-1}. The above band shifts, however, clearly suggest that MB dye molecules were bonded to BPAC.

3.2 Kinetics of adsorption

The sorption kinetics of MB on to BPAC are shown in Fig. 6a (symbols). It can be observed that the adsorption was found to be extremely rapid at the initial stage and slowed down as the adsorption proceeded. In the first 10 min, the percentages of total amounts adsorbed are about 95, 92, and 87 % for initial MB concentrations 800, 1,000, and 1,200 mg/L, respectively. This was attributed to the high concentration gradient in the beginning, which exhibited a high driving force for the migration of MB from solution to the surface of BPAC.

An adsorption kinetic study can also provide insights into the mechanisms involved in the adsorption process and the potential rate-controlling steps. To assess the adsorption kinetics of MB on BPAC, the experimental data were fitted to different kinetics models.

3.2.1 Pseudo-first-order model

The linear form of the Lagergren pseudo-first-order rate equation is generally expressed as follows [29]:

$$\ln(q_e - q_t) = \ln(q_e - k_1 t) \tag{5}$$

where q_e (mg g^{-1}) and q_t (mg g^{-1}) are the adsorption capacities at equilibrium and at time t, respectively. k_1 (min^{-1}) is the rate constant for pseudo-first-order adsorption. Plots of $\ln(q_e - q_t)$ versus t at various initial dye concentrations result in linear graphs with negative slopes (Fig. 6b). k_1 and q_e are calculated from the slopes and intercepts, respectively. In many cases, the first-order equation of Lagergren does not fit well with the whole range of contact time and is generally applicable over the initial stage of the adsorption processes [30]. Table 3 shows the correlation coefficients (R^2) changed in the range of 0.7767–0.8686, and the calculated q_e and the experimental q_e values do not agree. Therefore, the adsorption of MB dye onto BPAC does not follow the pseudo-first-order kinetics.

3.2.2 Pseudo-second-order model

The linear form of the pseudo-second-order kinetics model is expressed as follows [31]:

$$\frac{t}{q_t} = \frac{1}{k_2 q_e^2} + \frac{1}{q_e} t \tag{6}$$

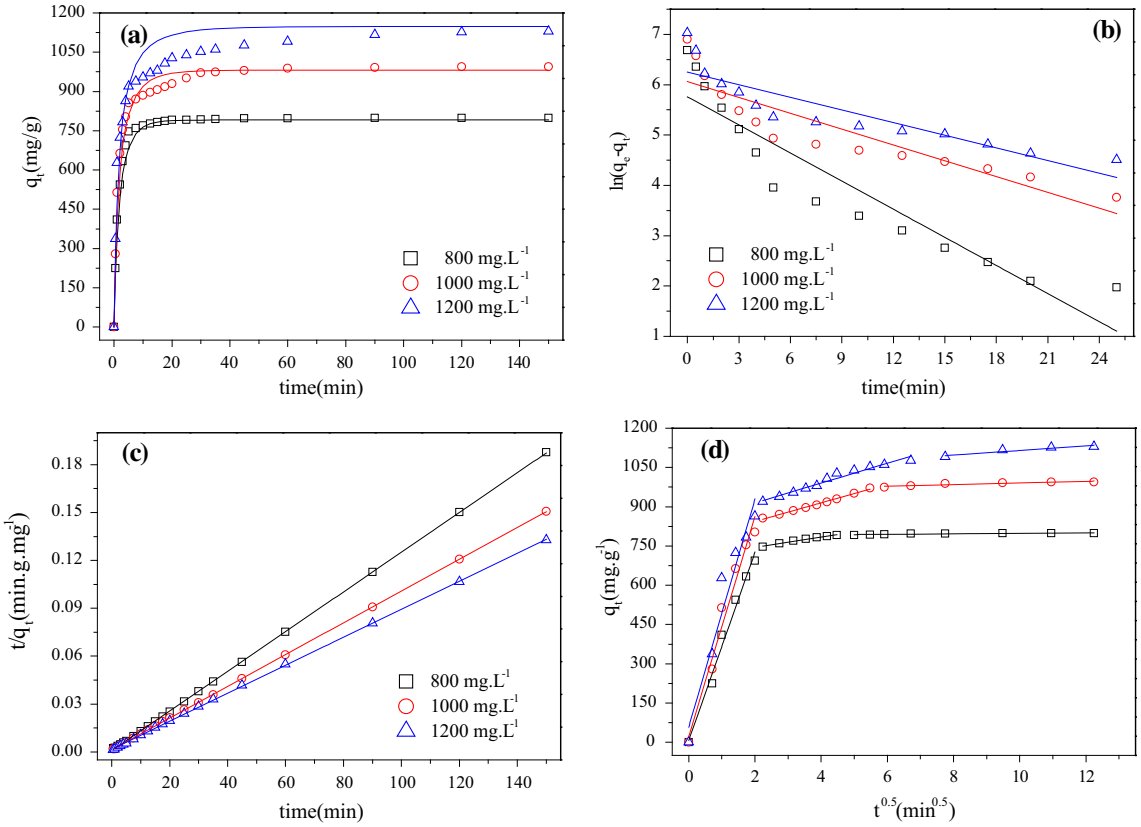

Fig. 6 **a** Effect of initial concentration and contact time on the adsorption of MB onto BPAC [The *symbols* are experimental data and *solid lines* are calculated values by Eq. (12)]. **b** Pseudo-first-order, **c** pseudo-second-order, and **d** intraparticle diffusion plots for MB adsorption by banana peel activated carbon at different concentrations

where k_2 (g mg^{-1} min^{-1}) is the rate constant of the second-order adsorption. Plots of t/q_t versus t result in linear graphs (Fig. 6c) from which q_e and k_2 were determined from the slopes and intercepts of the plot. Details are presented in Table 3 along with the corresponding correlation coefficients. This procedure can likely predict adsorption behavior. The linear plot shows the good agreement between the experimental and the calculated q_e values (Table 3). In addition, the values of corresponding correlation coefficients (R^2) for the pseudo-second-order kinetic model are high ($\geq$0.9998) for all MB concentrations, thus indicating the applicability of the pseudo-second-order kinetic model in describing the adsorption of MB on BPAC. These findings suggest that the rate-limiting step may be chemisorption related to valence forces through sharing or exchanging of electrons between adsorbate and adsorbent.

As shown in Table 3, the values of rate constants (k_1 and k_2), are found to decrease with increasing C_0, this result indicates that the main disadvantage of both pseudo-first-order and pseudo-second-order models is the dependency of their rate constants (k_1 and k_2) to the initial concentration of solute. Therefore the rate constants (k_1 and k_2) are really pseudo constants. This dependency has been shown both experimentally [32] and theoretically [33].

3.2.3 *Langmuir–Freundlich kinetic model*

One of the best models for analysis of adsorption kinetics is Eq. (7) which is also called Langmuir–Freundlich kinetic model [34, 35]:

$$\frac{d\theta subt}{dt} = k_a(C_0 - \beta\theta)\,(1-\theta)^n - k_d\theta_t^n \tag{7}$$

$$\beta = \frac{m_c q_m}{M_W V} \tag{8}$$

where $\theta_t = q_t/q_m$ is the surface fractional coverage of adsorbate at time t, C_0 is the initial concentration of solute, and k_a (M^{-1} min^{-1}) and k_d (min^{-1}) are the adsorption and desorption rate constants, respectively. q_m is the Langmuir–Freundlich maximum adsorption capacity, m_c is the mass of adsorbent, M_W is the molecular weight of adsorbate and V is the volume of solution. However, there is no analytical solution for this equation because of n exponent. Most recently Saeid Azizian [34] proposed an approximation

Table 3 Kinetic parameters for the adsorption of MB onto BPAC at different initial MB concentrations

Model parameter	Initial dye concentration (mg L^{-1})		
	800	1,000	1,200
Pseudo-first order			
q_e, (exp) (mg g^{-1})	799.12	994.54	1,130.15
k_1 (min^{-1})	0.186	0.105	0.084
q_e, (cal) (mg g^{-1})	317.43	431.20	517.75
R^2	0.8686	0.7960	0.7767
Pseudo-second order			
k_2 (g mg^{-1} min^{-1})	1.9×10^{-3}	7.6×10^{-4}	4.3×10^{-4}
q_e, (cal) (mg g^{-1})	806.45	1,005.02	1,141.44
R^2	0.9999	1	0.9998
Langmuir–Freundlich kinetic model			
k_0 (min^{-1})	0.3249	0.4064	0.4967
k_a (M^{-1} min^{-1})	190.86	187.65	188.32
k_d (min^{-1})	2.64×10^{-3}	2.59×10^{-3}	2.60×10^{-3}
Intraparticle diffusion model			
k_{id1} (mg g^{-1} $min^{-0.5}$)	359.43	419.05	435.32
k_{id2}	19.75	35.51	37.84
k_{id3}	0.95	3.15	8.80
C_1	7.26	23.32	58.40
C_2	705.20	772.81	839.16
C_3	788.74	959.38	1,026.99
$(R_1)^2$	0.9819	0.9667	0.9306
$(R_2)^2$	0.9825	0.9940	0.9619
$(R_3)^2$	0.7451	0.8302	0.8699

method for derivation of rate constants. This method was called "extended geometric method".

On the basis of this method for Eq. (7) the rate constant of adsorption (forward) can be computed by the following equation [35]:

$$k_a \cong \frac{k_0}{C_0\left(1-\frac{t_L}{2t_e}\right) - \beta k_0 t_L\left(\frac{1}{2}-\frac{n}{3}k_0 t_L + \frac{n(n-1)}{8}k_0^2 t_L^2\right)} \tag{9}$$

where k_0 is the initial slope of θ_t vs. t plot (linear region), t_L the initial time of adsorption where θ_t vs. t is linear, t_e the equilibrium time, n the exponent in Eq. (7) which can be easily found from the adsorption isotherm. So the input data of Eq. (9) can be easily obtained from the experimental data of θ_t vs. t and also adsorption isotherm. Desorption rate constant [k_d in Eq. (10)] can be easily computed by the following equation [36]:

$$k_d = \frac{k_a}{K} \tag{10}$$

where K is the Langmuir–Freundlich equilibrium constant. It is clear that for $n = 1$, Langmuir–Freundlich isotherm equation and Langmuir–Freundlich kinetic model convert to Langmuir isotherm and Langmuir kinetic model, respectively. In this case Eq. (9) simplifies to the following equation [34]:

$$k_a \cong \frac{k_0}{C_0\left(1-\frac{t_L}{2t_e}\right) - \beta k_0 t_L\left(\frac{1}{2}-\frac{1}{3}k_0 t_L\right)} \tag{11}$$

Equilibrium studies on the adsorption of MB onto BPAC showed that the present system obeys Langmuir isotherm and therefore $n = 1$, $q_m = 1{,}262.77$ mg g^{-1} and $K = 72{,}387.04$ M^{-1}. So we can estimate the k_a from Eq. (11). Some of the input data of Eq. (11) for the present system are $\beta = 3.377 \times 10^{-3}$ mol/l, $t_L = 1$ min and $t_e = 150$ min. The values of C_0, k_0 and the calculated k_a are listed in Table 3. These values show that k_0 is a function of C_0. The values of k_0 increase with increasing C_0. The values of k_a at different C_0 are in the same range and their small differences are due to experimental random error also approximations used in the method. Similar character was observed in the values of k_d at different C_0. So the average values of k_a and k_d for MB onto BPAC at room temperature are 188.94 M^{-1} min^{-1} and 2.61×10^{-3} min^{-1}, respectively. The interesting point is that the obtained rate constants are independent of initial concentration.

For checking the validity of results of extended geometric model it is useful to compare the calculated and experimental values of q at various times. For calculation of q for MB onto BPAC as a function of time for Langmuir kinetics is as follows [33, 34, 37]:

$$q = q_m \frac{\zeta e^{\tau+\lambda t} - \upsilon}{2a(1-e^{\tau+\lambda t})} \tag{12}$$

where

$$\lambda = \sqrt{b^2 - 4af} \tag{13}$$

$$\upsilon = \lambda \tag{14}$$

$$\zeta = b + \lambda \tag{15}$$

$$\tau = \ln\frac{\upsilon}{\zeta} \tag{16}$$

$$a = k_a\beta \tag{17}$$

$$b = -k_a\left(C_0 + \beta + \frac{1}{K}\right) \tag{18}$$

$$f = k_a C_0 \tag{19}$$

Equation (12) is an approximate equation for variation of q with time for Langmuir kinetics. By using the k_a and k_d from extended geometric method and also Eq. (12), variation of q with time can be calculated at different concentrations and are shown as solid lines in Fig. 6a. As shown in this figure the agreement between calculated and experimental q values is good for the lower C_0. However,

the calculated and experimental values did not match completely for higher C_0 and at time more than 5 min, when the most significant deviations can be seen. The reason for these deviations are (1) two approximations in extended geometric method (2) the use of the average value of k_a and k_d for all concentrations (3) experimental errors and (4) adsorbate–adsorbate interactions [34, 38].

It is interesting to note that for finding of rate constants with extended geometric method, one just needs initial kinetic data. Also by using the Langmuir–Freundlich kinetic model and calculated rate constants, it is possible to predict the variation of q with time in the whole region: from short initial times to long times when the system is close to equilibrium for different initial concentrations. The results of kinetic modeling suggested that the removal of MB by BPAC is chemisorption controlled.

3.2.4 Intraparticle diffusion model

The diffusivity of the solute molecules has an important effect on the total rate of an adsorption process. The results acquired from the pseudo-second-order kinetic model or Langmuir–Freundlich kinetic model are not sufficient to predict the diffusion mechanism. The adsorbate transfer from solution phase to the surface of the adsorbent molecules may be controlled either by one or more steps, e.g., film or external diffusion, pore diffusion, surface diffusion, and adsorption on the pore surface, or by a combination of more than one step. The intraparticle diffusion model is generally expressed as follows [39]:

$$q_t = k_{id} t^{0.5} + C \tag{20}$$

where q_t is the amount of MB adsorbed (mg g^{-1}) at time t, and k_{id} is the intraparticle diffusion rate constant (mg g^{-1} $min^{-0.5}$). The value of intercept of the plot (C) reflects the thickness of the boundary layer, the larger the intercept the greater the boundary layer effect. If intraparticle diffusion occurs, then q_t versus $t^{0.5}$ will be linear and if the plot passes through the origin, then the rate limiting step is only due to the intraparticle diffusion. Otherwise, some other mechanism along with intraparticle diffusion is also involved [40]. In most cases, this plot gives general features of three stages: initial curved portion, followed by an intermediate linear portion and a plateau. The initial sharper, is due to the instantaneous adsorption or external surface adsorption (external mass transfer). The intermediate linear part is due to intraparticle diffusion and the plateau to the equilibrium stage where intraparticle diffusion starts to slow down due to extremely low solute concentrations in the solution [41].

As can be seen from Fig. 6d, the data points are related by three stages. The initial curve portion is due to the instantaneous adsorption or external surface adsorption. The second linear portion is due to intraparticle diffusion and the third linear portion is the final equilibrium Stage. The slope of the second linear portion characterizes the rate parameter corresponding to the intraparticle diffusion, whereas the intercept of this portion is proportional to the boundary layer thickness. The calculated k_{id2} values for each initial concentration are given in Table 3. It was found that the rate constant increased with increasing initial MB concentrations, implies that the increased driving force at high initial concentrations promotes the intraparticle diffusion of the adsorbate onto the adsorbent [42]. The correlation coefficients $(R_2)^2$ for the intraparticle diffusion model are between 0.9619 and 0.9940 (Table 3), indicating that adsorption of MB dye onto BPAC may be controlled by an intraparticle diffusion model. Although all the intraparticle diffusion plots for various initial dye concentrations show a linear relationship, no line segment passed through the origin. The deviation was due to the differences in mass transfer rate in the initial and final stages of adsorption [43]. All C values have positive and increase with increasing the MB concentrations. The results show that MB adsorption control with not only the intraparticle diffusion but also the film diffusion [41].

3.3 Thermodynamic study

The influence of temperature on the adsorption capacity of BPAC with regard to MB adsorption is depicted in Fig. 7a. Maximum equilibrium sorption capacity was acquired at 318 K. A slight increase in the adsorption capacity of MB occurred as temperature increased, thus demonstrating that the adsorption reaction is endothermic in nature, and that the adsorption of MB by BPAC may involve not only physical but also chemical sorption [27]. A similar trend was observed with the use of banana stalk-based activated carbon for the sorption of malachite green dye previously by others [44] supporting the present results.

To understand the thermodynamic performances of MB adsorption onto BPAC, thermodynamic functions were evaluated. Thermodynamic parameters, i.e., the change in the Gibbs free energy (ΔG^0, kJ mol^{-1}), the change in enthalpy (ΔH^0, kJ mol^{-1}), and the change in entropy (ΔS^0, J mol^{-1} K^{-1}), are used to evaluate the thermodynamic feasibility and the nature of the process. The ΔG^0, ΔH^0, and ΔS^0 parameters were determined using Eqs. (21)–(23) and are listed in Table 4.

$$k_d = \frac{C_{Ae}}{C_e} \tag{21}$$

$$\Delta G^0 = -RT \ln k_d \tag{22}$$

$$\ln k_d = \frac{\Delta S^0}{R} - \frac{\Delta H^0}{RT} \tag{23}$$

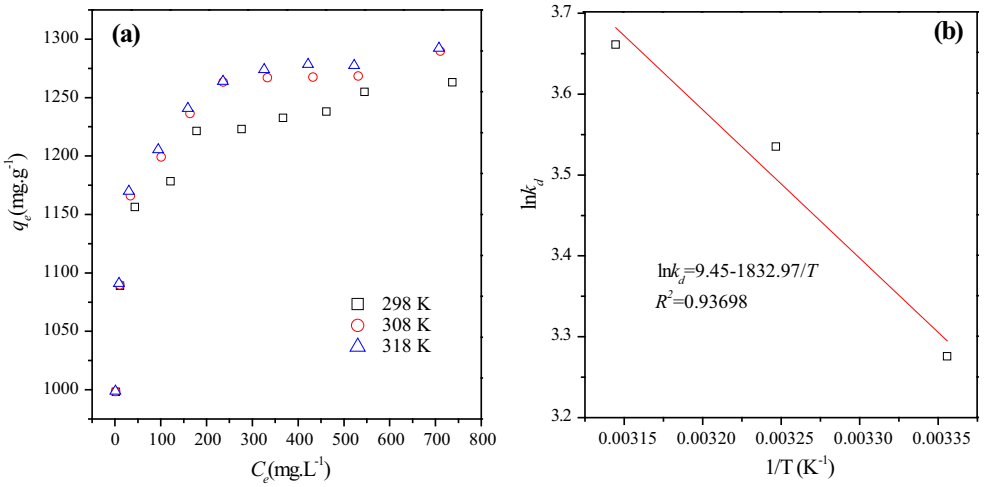

Fig. 7 **a** Effect of temperature on the adsorption of MB dye onto banana peel activated carbon (BPAC). **b** Plot of ln k_d versus 1/T for MB dye adsorption by BPAC

Table 4 Thermodynamic parameters for the adsorption of MB onto BPAC at different temperatures

Temperature (K)	k_d (L mol^{-1})	ΔG^0 (kJ mol^{-1})	ΔH^0 (kJ mol^{-1})	ΔS^0 (J mol^{-1} K^{-1})
298	26.46	−8.116		
308	34.30	−9.052	15.13	0.078
318	38.91	−9.680		

where C_{Ae} (mg L^{-1}) is the concentration of MB adsorbed on BPAC at equilibrium, C_e (mg L^{-1}) is the equilibrium concentration of MB in bulk solution, T is the solution temperature in Kelvin, k_d is the equilibrium constant, and R is the gas constant (8.314 J mol^{-1} K^{-1}). The value of k_d in the lowest experimental dye concentration can, therefore, be obtained. ΔH^0 and ΔS^0 were obtained from the slope and intercept of the van't Hoff plots of ln k_d versus *1/T* (Fig. 7b). Table 4 shows the calculated data. The negative values of ΔG^0 verify the feasibility and spontaneity of the adsorption of MB dye on BPAC. Additionally, the value of ΔG^0 changed from −8.116 to −9.680 kJ mol^{-1}, whereas the temperature increased from 298 to 318 K, thus suggesting that adsorption is highly spontaneous at higher temperatures. The positive values of ΔH^0, further confirm the endothermic nature of the adsorption process and the possibility of physical adsorption. These findings are in agreement with the obtained isotherm results. The positive values of ΔS^0 suggest the occurrence of increased randomness at the solid solution interface with some structural changes in the adsorbate and adsorbent as well as the good affinity of BPAC for the MB dye. The increase in dye adsorption with increasing temperature may also be caused by the enhanced rate of intraparticle diffusion of the adsorbate, as diffusion is an endothermic process [45].

4 Conclusions

BPAC was synthesized for the first time with a very high surface area of 1,950 m^2 g^{-1} and was used to remove dye (MB or Orange II) from aqueous solutions. Results of adsorption experiments showed that the BPAC exhibited high adsorption capacity toward MB, a cationic dye. The equilibrium MB adsorption data were best described by the Langmuir isotherm model and the adsorption kinetics can be successfully fitted to pseudo-second-order kinetic model. The results of the intraparticle diffusion model suggest intraparticle diffusion was not the only rate-controlling step. The thermodynamic studies established the spontaneous and endothermic nature of MB adsorption. Banana peel is therefore a promising raw material in the production of activated carbon for the effective removal of cationic dye contaminants such as MB dye.

Acknowledgments This work was supported by the National Natural Science Foundation of China (Grant No. 21477009), the Project Funded by the Priority Academic Program Development of Jiangsu Higher Education Institutions and Technology Innovation Team of Colleges, and the Universities-Funded Project of Jiangsu Province (No. 2011-24).

References

1. M. Simonič, A. Lobnik, Desalination **271**, 219 (2011)
2. C.S.D. Rodrigues, L.M. Madeira, R.A.R. Boaventura, Environ. Technol. **34**, 719 (2013)

3. Y. Al-Ani, Y.L. Li, J. Taiwan Inst. Chem. Eng. **43**, 942 (2012)
4. C. Benincá, P. Peralta-Zamora, C.R.G. Tavares, L. Igarashi-Mafra, Ozone Sci. Eng. **35**, 295 (2013)
5. B.K. Körbahti, J. Hazard. Mater. **145**, 277 (2007)
6. B. Bakheet, S. Yuan, Z.X. Li, H.J. Wang, J.N. Zuo, S. Komarneni, Y.J. Wang, Water Res. **47**, 6234 (2013)
7. S. Raghu, C. Ahmed, Basha. J. Hazard. Mater. **149**, 324 (2007)
8. S. Mondal, H. Ouni, M. Dhahbi, S. De, J. Hazard. Mater. **229–230**, 381 (2012)
9. S. Chakraborty, S. De, S. DasGupta, J.K. Basu, Chemosphere **58**, 1079 (2005)
10. H. Cherifi, B. Fatiha, H. Salah, Appl. Surf. Sci. **282**, 52 (2013)
11. D. Angin, T.E. Kose, U. Selengil, Appl. Surf. Sci. **280**, 705 (2013)
12. M.S. Sajab, C.H. Chia, S. Zakaria, P.S. Khiew, Bioresour. Technol. **128**, 571 (2013)
13. B.H. Hameed, F.B.M. Daud, Chem. Eng. J. **139**, 48 (2008)
14. Y.F. Feng, H. Zhou, G.H. Liu, J. Qiao, J.H. Wang, H.Y. Lu, L.Z. Yang, Y.H. Wu, Bioresour. Technol. **125**, 138 (2012)
15. F. Ahmad, W.M.A.W. Daud, M.A. Ahmad, R. Radzi, Chem. Eng. Res. Des. **90**, 1480 (2012)
16. C.A. Basar, J. Hazard. Mater. **135**, 232 (2006)
17. G. Cimino, R.M. Cappello, C. Caristi, G. Toscano, Chemosphere **61**, 947 (2005)
18. K.A.G. Gusmao, L.V.A. Gurgel, T.M.S. Melo, L.F. Gil, Dyes Pigment. **92**, 967 (2012)
19. M.M. El Jamal, M.C. Ncibi, Acta Chim. Slov. **59**, 24 (2012)
20. S. Sircar, T.C. Golden, M.B. Rao, Carbon **34**, 1 (1996)
21. S.K. Das, J. Bhowal, A.R. Das, A.K. Guha, Langmuir **22**, 7265 (2006)
22. W.E. Rashwan, B.S. Girgis, Adsorpt. Sci. Technol. **22**, 181 (2004)
23. O. Pezoti Jr, A.L. Cazetta, I.P.A.F. Souza, K.C. Bedin, A.C. Martins, T.L. Silva, V.C. Almeida, J. Ind. Eng. Chem. **20**, 4401 (2014)
24. C. Hsiu-Mei, C. Ting-Chien, P. San-De, H.-L. Chiang, J. Hazard. Mater. **161**, 1384 (2009)
25. K.S.W. Sing, D.H. Everett, R.A.W. Haul, L. Moscou, R.A. Pierotti, J. Rouquerol, T. Siemieniewska, Pure Appl. Chem. **57**, 603 (1984)
26. P.J. Branton, K.S.W. Sing, J.W. White, J. Chem. Soc., Faraday Trans. **93**, 2337 (1997)
27. S. Chen, J. Zhang, C. Zhang, Q. Yue, Y. Li, C. Li, Desalination **252**, 149 (2010)
28. K.R. Hall, L.C. Eagleton, A. Acrivos, T. Vermeulen, Ind. Eng. Chem. Fundam. **5**, 212 (1966)
29. I.A.W. Tan, A.L. Ahmad, B.H. Hameed, J. Hazard. Mater. **154**, 337 (2008)
30. B.H. Hameed, A.L. Ahmad, K.N.A. Latiff, Dyes Pigment. **75**, 143 (2007)
31. Y.S. Ho, G. McKay, Process Biochem. **34**, 451 (1999)
32. F. Al Mardini, B. Legube, J. Hazard. Mater. **170**, 754 (2009)
33. S. Azizian, J. Colloid Interface Sci. **276**, 47 (2004)
34. S. Azizian, M. Haerifar, J. Basiri-Parsa, Chemosphere **68**, 2040 (2007)
35. C.W. Cheung, J.F. Porter, G. McKay, Sep. Purif. Technol. **19**, 55 (2000)
36. G. Crini, H. Peindy, F. Gimbert, C. Robert, Sep. Purif. Technol. **53**, 97 (2007)
37. S. Azizian, M. Haerifar, H. Bashiri, Chem. Eng. J. **146**, 36 (2009)
38. M.-L. Lin, Z.-W. Zhao, F.-Y. Cui, S. Xia, Desalin. Water Treat. **44**, 245 (2012)
39. W.J. Weber, J.R. Moris, J. San, Eng. Div. ASCE Civil Eng. **89**, 31 (1963)
40. Y. Sun, Q. Yue, B. Gao, Q. Li, L. Huang, F. Yao, X. Xu, J. Colloid Interface Sci. **368**, 521 (2012)
41. T. Depci, Chem. Eng. J. **181–182**, 467 (2012)
42. I.A. Tan, A.L. Ahmad, B.H. Hameed, J. Hazard. Mater. **164**, 473 (2009)
43. T. Depci, A.R. Kul, Y. Önal, Chem. Eng. J. **200–202**, 224 (2012)
44. O.S. Bello, M.A. Ahmad, N. Ahmad, Chem. Ecol. **28**, 153 (2011)
45. S. Wang, Y. Boyjoo, A. Choueib, Z.H. Zhu, Water Res. **39**, 129 (2005)